CO_2 Reduction

Deutsche Ausgabe: DOI: 10.1002/ange.201601038
Internationale Ausgabe: DOI: 10.1002/anie.201601038

Electrocatalytic and Solar-Driven CO_2 Reduction to CO with a Molecular Manganese Catalyst Immobilized on Mesoporous TiO_2

*Timothy E. Rosser[+], Christopher D. Windle[+], and Erwin Reisner**

Abstract: *Electrocatalytic CO_2 reduction to CO was achieved with a novel Mn complex, fac-[MnBr(4,4′-bis(phosphonic acid)-2,2′-bipyridine)$(CO)_3$] (**MnP**), immobilized on a mesoporous TiO_2 electrode. A benchmark turnover number of 112 ± 17 was attained with these TiO_2 | **MnP** electrodes after 2 h electrolysis. Post-catalysis IR spectroscopy demonstrated that the molecular structure of the **MnP** catalyst was retained. UV/vis spectroscopy confirmed that an active Mn–Mn dimer was formed during catalysis on the TiO_2 electrode, showing the dynamic formation of a catalytically active dimer on an electrode surface. Finally, we combined the light-protected TiO_2 | **MnP** cathode with a CdS-sensitized photoanode to enable solar-light-driven CO_2 reduction with the light-sensitive **MnP** catalyst.*

The reduction of CO_2 to CO is viewed as a potentially lucrative and renewable source of a key chemical feedstock, as well as a strategy to reduce rising atmospheric CO_2 levels. Electrocatalysis by molecular transition-metal complexes is a viable means of achieving this transformation, typically offering excellent tunability[1] and selectivity[2] as well as providing opportunities to study the catalytic mechanism.[3] Alternatives based on inexpensive solid-state materials usually offer less well-defined catalytic centers that prevent a detailed understanding of the catalytic mechanism.[4]

Immobilization of such molecular catalysts on electrode surfaces makes efficient use of the active metal centers and therefore enables a true appraisal of properties, such as the turnover number (TON).[5] However, in most cases reported to date, molecular catalysts were deposited on carbon[5c,6] and Pt-based[7] electrodes. These offer low transparency to visible light, and only in very few cases have the surface-bound catalytic intermediates been characterized spectroscopically in situ.[2c,8] Bimolecular reaction mechanisms, in which active dimers form during catalysis, have not been observed on electrode surfaces, and it has been thought that such mechanisms would be impeded by immobilization of a monomeric pre-catalyst.[5b,9]

First-row transition-metal complexes based on [MnBr$(CO)_3$(L)] (L = bipyridine and derivatives) have emerged in recent years as promising electrocatalysts for CO_2 reduction owing to their high selectivity and low overpotential for catalysis.[10] They also contain only Earth-abundant elements, which is a significant advantage over analogous Re-based catalysts.[7b,8,11] The low overpotential is a direct consequence of the bimolecular reaction mechanism, whereby a Mn^0—Mn^0 dimer is formed after the first reduction of the homogeneous molecular catalyst, which then reduces CO_2 to CO (L = 4,4′-dimethyl-2,2′-bipyridine).[10a] However, the maximum TONs achieved by this class of complex for electrocatalytic CO production are 34 after 18 h,[10a] and 36 after 6 h.[12] Mn catalysts have been integrated onto electrodes in polymer films, such as Nafion, where they reached a TON of 14 based on the total amount of catalyst used.[13] From electrochemical measurements it was proposed that the Mn^0–Mn^0 dimer forms in the polymer matrix, although this was not spectroscopically verified. Preliminary studies of an electro-polymerized pyrrole-based Mn catalyst deposited on silicon nanowires have also suggested photoelectrochemical (PEC) CO_2 reduction, based on cyclic voltammetry (CV) results.[14]

Herein, we present a novel Mn^I CO_2 reduction electrocatalyst with a phosphonate functionality (**MnP**, Scheme 1) that allows anchoring and direct wiring between the catalytic center and a metal oxide surface,[15] as has been achieved for an analogous phosphonate-modified Re complex.[16] We employ a mesoporous TiO_2 electrode, because it offers 1) long-term stability and conductivity under reducing conditions,[17] 2) a three-dimensional morphology for high cata-

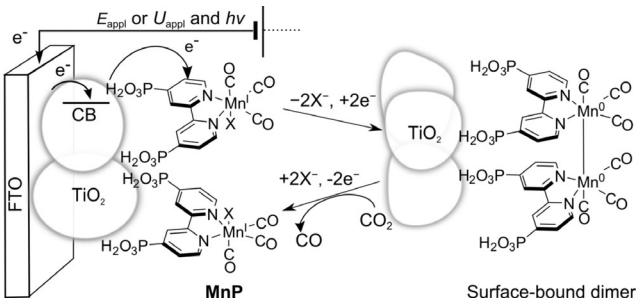

Scheme 1. Schematic representation and proposed mechanism for CO_2 reduction by TiO_2 | **MnP** (X = Br^- in the isolated compound).

[*] T. E. Rosser,[+] Dr. C. D. Windle,[+] Dr. E. Reisner
Christian Doppler Laboratory for Sustainable SynGas Chemistry
Department of Chemistry
University of Cambridge
Lensfield Road, Cambridge, CB2 1EW (UK)
E-mail: reisner@ch.cam.ac.uk
Homepage: http://www-reisner.ch.cam.ac.uk/
[+] These authors contributed equally to this work.

Supporting information and ORCID(s) from the author(s) for this article are available on the WWW under http://dx.doi.org/10.1002/anie.201601038. Open data related to this publication is available at the University of Cambridge data repository (http://www.repository.cam.ac.uk/handle/1810/254575).

lyst loading and to facilitate close inter-molecular interactions, and 3) transparency for spectroelectrochemical characterization of catalytic intermediates.[18] The electrochemical investigations establish the heterogenized **MnP** as the best-performing Mn electrocatalyst to date, which was enabled by a dynamic TiO_2|**MnP** interface and dimerization of the immobilized Mn catalyst. Finally, we present the first example of CO_2 reduction by a Mn catalyst driven by full UV/Vis solar-spectrum irradiation, circumventing the typical photo-instability[13b,19] of these compounds by combining the TiO_2|**MnP** hybrid cathode in the dark with a CdS-sensitized photoanode.

MnP (Scheme 1) was synthesized by coordination of 4,4′-bis(phosphonic acid)-2,2′-bipyridine to pentacarbonyl manganese(I) bromide in ethanol under N_2 while protected from light. The product was isolated as an orange solid in 63% yield and characterized by CHNP microanalysis, ^{31}P-NMR spectroscopy, high-resolution mass spectrometry, and infrared (IR) spectroscopy ($\tilde{\nu}_{CO} = 2030$, 1946, and 1930 cm^{-1}, Figure 1a), which confirmed a *fac*-Mn tricarbonyl species.[19] Full synthetic and characterization details can be found in the Supporting Information. **MnP** was insoluble in CH_3CN and therefore characterized by CV in DMF (Figure S1 in the Supporting Information). A catalytic wave at $E_{onset} = -1.8$ V versus Fc^+/Fc ($Fc = [(\eta\text{-}C_5H_5)_2Fe]$) was observed when H_2O was added and the cell was purged with CO_2. The presence of water in the electrolyte solution is known to significantly increase electrocatalytic CO_2 reduction activity, by allowing the Mn–Mn dimer to directly react with CO_2.[10a]

Mesoporous TiO_2 electrodes were prepared by a doctor-blading procedure, applying a suspension of commercial P25 TiO_2 nanoparticles (anatase/rutile (8/2) mixture, average particle size 21 nm) to a fluorine-doped tin oxide (FTO) coated glass electrode, and further experimental details can be found in the Supporting Information. Scanning electron microscopy (SEM) on the resultant electrode revealed a mesoporous film with a thickness of approximately 6 μm (Figure S2a). Loading of the catalyst onto the TiO_2 electrode was achieved by drop-casting a methanol solution of **MnP**, resulting in 34 nmol Mn per cm^2 of geometrical surface area. The presence of IR bands at $\tilde{\nu}_{CO} = 2032$ and 1928 cm^{-1} in the attenuated total reflectance Fourier transform infrared (ATR-FTIR) spectrum confirmed the presence of **MnP** on the electrode (TiO_2|**MnP**; Figure 1a). Immobilization and electronic communication of the **MnP** with a metal oxide was confirmed by adsorbing **MnP** on conducting and mesoporous tin-doped indium oxide (ITO) electrodes instead (film thickness approximately 7 μm, see Figure S2b and Supporting Information for experimental details). CV with ITO|**MnP** in anhydrous CH_3CN (1.0 M Bu_4NBF_4) displayed a reversible wave at $E = -1.6$ V versus Fc^+/Fc, assigned to the reduction of Mn^I to Mn^0. The peak current was linearly dependent on the scan rate, indicative of an immobilized species in good electronic communication with the electrode (Figure S3).

TiO_2 becomes conductive at potentials more negative than the conduction band (CB), thus the CV of TiO_2|**MnP** can be employed to study electrocatalytic CO_2 reduction. The CV scan of a bare (Mn-free) TiO_2 electrode in CH_3CN/H_2O (19/1, 0.1 M Bu_4NBF_4) shows the filling and emptying of the conduction band of TiO_2 (Figure 1b), as confirmed by the increase in absorbance in the $\lambda = 600$–850 nm region of the electronic spectrum at an applied potential, E_{appl}, of −1.8 V versus Fc^+/Fc (Figure S4).[17b,20] Comparable CV features are observed with a bare TiO_2 electrode under CO_2 or TiO_2|**MnP** under N_2. However, TiO_2|**MnP** purged with CO_2 showed an increased current with an onset of $E = -1.6$ V versus Fc^+/Fc, indicative of electrocatalytic CO_2 reduction by the heterogenized **MnP** catalyst (Figure 1b). Furthermore, the ratio of cathodic to anodic charge in the forward and reverse CV scans increased from approximately 1:1 to 4:1 by changing TiO_2 to TiO_2|**MnP** under CO_2, suggesting that conduction-band electrons of TiO_2 are consumed by the Mn catalyst on the CV timescale and are therefore unavailable for discharging during the anodic scan.

The increased current arising from TiO_2|**MnP** under CO_2 was confirmed as being the result of the reduction of CO_2 to CO by controlled-potential electrolysis (CPE). Figure 2a shows the gaseous products formed when TiO_2|**MnP** electrodes were held at $E_{appl} = -1.7$ V versus Fc^+/Fc in the dark under CO_2, and monitored by gas chromatography (GC). After 2 h, an average of 1.10 ± 0.25 C was passed, with the production of 3.75 ± 0.56 μmol CO, corresponding to a Faradaic efficiency (FE) of 67 ± 5%. The FE for H_2 production was 12.4 ± 1.4%, and the formation of formate was not detectable by ion chromatography. The TON_{CO} of 112 ± 17 was calculated based on the amount of **MnP** drop-cast onto the electrode, and is thus a lower limit since it assumes all **MnP** remains bound and active throughout CPE. This is the highest TON_{CO} based on the total amount of catalyst used for a Mn catalyst in CO production, and was achieved at a low overpotential (η) of approximately 0.42 V, calculated using a standard potential for CO_2 reduction to CO ($E^{0'}(CO_2/CO)$) of −1.28 V versus Fc^+/Fc in these conditions.[21] This is one of the lowest overpotentials observed for a transition-metal-based catalyst in non-aqueous solution,[1a,2a,22] matched only by a modified Fe-porphyrin in homogeneous DMF solution ($\eta = 0.41$ V)[21a] and a Mn catalyst that achieved a TON_{co} of 36 after 6 h ($\eta = 0.35$ V).[12]

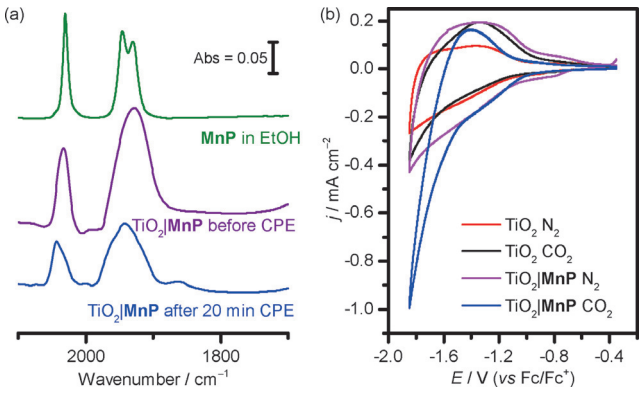

Figure 1. a) Solution FTIR of **MnP** and ex situ ATR-FTIR spectra of TiO_2|**MnP** before and after controlled-potential electrolysis (CPE) for 20 min at $E_{appl} = -1.7$ V versus Fc^+/Fc. b) CV scans of TiO_2 and TiO_2|**MnP** (geometrical surface area = 1.0 cm^2) under N_2 and CO_2. Conditions: CH_3CN/H_2O (19/1), 0.1 M Bu_4NBF_4, $\nu = 100$ $mV s^{-1}$, Ag/AgCl reference electrode (RE), Pt counter electrode (CE), room temperature.

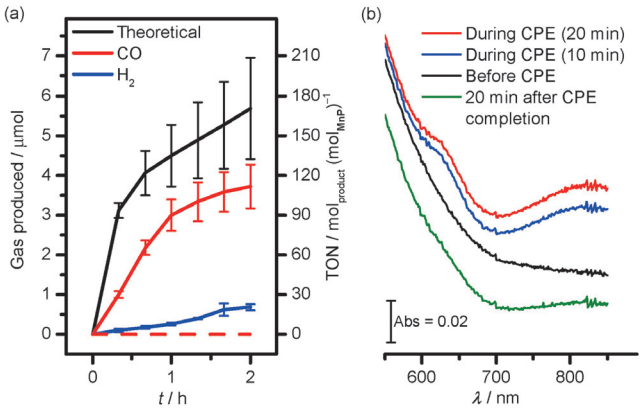

Figure 2. a) Electrocatalytic CO production by TiO_2|**MnP** (solid lines) performed with $E_{appl} = -1.7$ V versus Fc^+/Fc for 2 h, and theoretical maximum based on charge passed in the CPE. Dashed lines show no CO production in the absence of **MnP** or CO_2. b) In situ UV/Vis spectroelectrochemistry of TiO_2|**MnP** under CPE at $E_{appl} = -1.7$ V versus Fc^+/Fc for 20 min. Lower wavelength data are not shown because of strong scattering from the mesoporous TiO_2. CPE conditions: CH_3CN/H_2O (19/1, 0.1 M Bu_4NBF_4, Pt CE, Ag/AgCl RE) under CO_2 at room temperature.

TiO_2|**MnP** exhibited good CO selectivity, with a CO:H_2 ratio of approximately 12:1 after 1 h CPE, although this ratio was reduced to 5.4:1 after 2 h, presumably a result of desorption or degradation of the Mn catalyst during the second hour of electrolysis. In the absence of either CO_2 or the Mn catalyst (Figures S5a and S5b), no CO was produced. H_2 production by bare TiO_2 was 1.91 ± 0.31 µmol after 2 h, compared to 1.43 ± 0.22 µmol for TiO_2|**MnP** with a surface coverage of 22 nmol cm^{-2} and 0.69 ± 0.08 µmol with a coverage of 34 nmol cm^{-2} (see Figure 2a, Figure S5, and Table S1). Increasing amounts of **MnP** on TiO_2 therefore suppress H_2 in favor of CO production, suggesting that H_2 production by TiO_2|**MnP** may originate from unmodified areas of the TiO_2 rather than the catalyst itself.

IR and UV/Vis spectroscopies confirmed the molecular nature of **MnP** during catalysis on TiO_2. Figure 1a shows an ATR-FTIR spectrum of TiO_2|**MnP** taken after CPE for 20 min ($Q = 0.37$ C, approximate $TON_{CO} = 34$), revealing peaks at $\tilde{\nu}_{CO} = 2042$ and 1943 cm^{-1}. These vibrational CO stretches closely match the spectrum of the as-prepared electrode, with a slight shift explained by exchange of coordinated Br^- for a solvent molecule, and therefore demonstrate that the molecular structure of the catalyst remains largely unchanged during catalytic turnover. Deactivation of the Mn catalyst to a material that is no longer molecular would be unlikely to give high CO selectivity, corroborating Figure 2a.

The UV/Vis spectra of TiO_2|**MnP** before, during, and after 20 min CPE with $E_{appl} = -1.7$ V versus Fc^+/Fc are shown in Figure 2b. During CPE, bands at 630 and 820 nm were observed, which are assigned to the formation of an Mn–Mn dimer by comparison to similar peaks formed during homogeneous CPE of the unmodified [MnBr(bpy)$(CO)_3$] (Table S2 for assignment).[1a,2b] We excluded the formation of the mononuclear doubly reduced **MnP** anion, analogues of which are also known to reduce CO_2 when dimer formation is impeded,[1b,2c] due to the lack of a strong peak at approximately 548 nm as found in an analogous Mn compound in THF[3a] (difference spectrum in Figure S6). After CPE for 20 min, the TiO_2|**MnP** was left under CO_2 without an applied potential, and the peaks resulting from the dimer were lost (Figure 2b). This was corroborated by the IR spectrum in Figure 1a, which indicated mainly the presence of the Mn^I monomer, but with a small peak at 1865 cm^{-1} and a broadening of the peak at 1943 cm^{-1}, assigned to a small amount of remaining dimer.[3b] These data are consistent with the mechanism shown in Scheme 1, with the formation of a steady-state concentration of the catalytically active Mn–Mn dimer. This intermediate then reacts with CO_2 before it can be identified ex situ, reforming the Mn^I monomer as detected in the IR spectrum.

Immobilization of **MnP** on mesoporous TiO_2 creates a high local concentration of Mn^0 under reducing conditions at the electrode surface. Phosphonic acid modified molecules, such as **MnP**, display some lability when bound to TiO_2,[23] and phosphate buffer has been used to displace anchored catalysts from TiO_2 particles, demonstrating a dynamic interaction.[24] We propose that the high activity and low overpotential of this system is due to either temporary desorption of the catalyst, followed by dimerization and re-anchoring within mesoporous TiO_2, or the high local concentration of **MnP** placing the metal centers in an environment where they are predisposed to dimerization upon reduction.

Manganese carbonyl compounds, such as **MnP**, show instability under illumination,[19] and tend to undergo photolysis and release CO ligands.[25] Consequently, the few reports of Mn-based CO_2 reduction photocatalysis use monochromatic or narrowly filtered light to prevent decomposition of the catalyst.[14,25a,26] This photo-instability was observed for TiO_2|**MnP**, which displayed a significantly lower CO production of 0.39 ± 0.16 µmol (12 ± 3% FE) when CPE was performed under UV-filtered 1 sun illumination ($\lambda > 420$ nm to avoid TiO_2 band-gap excitation in this experiment) at -1.7 V versus Fc^+/Fc for 2 h (Figure S7). The significant H_2 production (1.74 ± 0.6 µmol, 59 ± 8% FE) is consistent with degradation of **MnP** and possibly the formation of a catalytically active Mn deposit. Therefore, TiO_2|**MnP** cannot be used directly in a CO_2 reducing photocathode that efficiently absorbs sunlight and exposes the catalyst to irradiation.

An alternative strategy to drive CO_2 reduction using full solar-spectrum irradiation was implemented, integrating **MnP** into a photoelectrochemical circuit with a photoanode, wired to TiO_2|**MnP**, which was kept in the dark. CdS-sensitized ZnO nanosheet electrodes were prepared following a reported procedure (SEM in Figure S8a),[27] which absorb a broad spectrum of light below 530 nm according to the electronic spectrum shown in Figure S8b. These ZnO|CdS electrodes gave an anodic photocurrent in the presence of triethanolamine (TEOA) as a hole scavenger with an onset of -1.65 V versus Fc^+/Fc, a potential at which TiO_2|**MnP** gives a cathodic current from CO_2 reduction (Figure 3a). The linear-sweep voltammetry (LSV) scan of a two-electrode, two-compartment PEC cell comprising a CdS|ZnO photoanode and a TiO_2|**MnP** cathode (kept in the dark) in Figure 3b shows a small photocurrent at zero bias, which

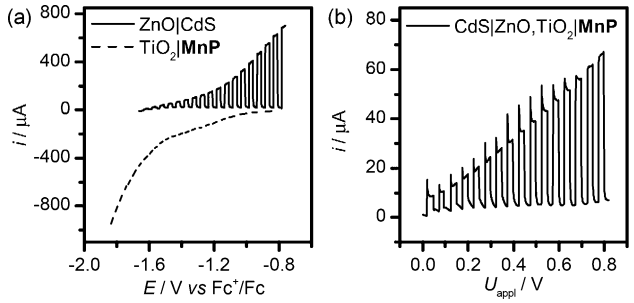

Figure 3. a) Three-electrode LSV scans of ZnO | CdS and TiO_2 | **MnP** (Ag/AgCl RE, Pt CE). b) LSV scans of ZnO | CdS and TiO_2 | **MnP** in a two-electrode configuration. Conditions: CH_3CN/H_2O (19/1, 0.1 M Bu_4NBF_4, 0.1 M TEOA (except three-electrode TiO_2 | **MnP**), purged with CO_2), simulated solar irradiation (AM 1.5 G, 100 mW cm^{-2}), TiO_2 | **MnP** kept in the dark, room temperature.

increased as a bias potential (U_{appl}) was applied. To confirm that CO was produced, we performed CPE in a two-electrode configuration in CH_3CN/H_2O electrolyte solution (19/1, 0.1 M Bu_4NBF_4, 0.1 M TEOA, purged with CO_2). An applied potential of 0.6 V for 1 h passed a charge of 0.26 C, and 0.36 ± 0.07 μmol of CO (26 % FE, 2.6:1 CO:H_2 ratio, $TON_{CO} = 11$, Figure S9) was measured. The lower CO production performance compared to the three-electrode electrocatalytic system could be due to the potentially disruptive presence of TEOA in the electrolyte solution, the lower charge passed and the different potential at the cathode. Nevertheless, this is the first example of full spectrum solar-light driven CO_2 reduction with a Mn catalyst.

In conclusion, we have presented **MnP** as a novel Mn-based CO_2 reduction catalyst that allows immobilization onto a mesoporous TiO_2 electrode with its phosphonic acid anchoring groups. The TiO_2 | **MnP** cathode achieved efficient CO_2 reduction to CO, reaching an unprecedented TON_{CO} of 112 ± 17 at an overpotential of 0.42 V after 2 h CPE. During electrocatalytic CO_2 reduction, a Mn–Mn dimer was formed, which is an important catalytic intermediate in homogeneous solution. This is, to our knowledge, the first observation of the dynamic formation of active catalytic dimers on a surface, providing a strategy for retaining homogeneous reaction mechanisms whilst also gaining the advantages of heterogeneous catalysis. Finally, we utilized the CO_2 reduction activity of TiO_2 | **MnP** at a low overpotential to assemble a PEC cell with a CdS-sensitized photoanode, demonstrating that Mn catalysts can be used in solar-driven CO_2 reduction in spite of their photo-instability. This work represents an advance in moving molecular CO_2 reduction electrocatalysis towards a full artificial photosynthetic system. This was achieved through the immobilization of the catalyst, attainment of a high TON at low overpotential, and implementation of a PEC cell.

Acknowledgements

We gratefully acknowledge financial assistance from the EPSRC, the Christian Doppler Research Association (Austrian Federal Ministry of Science, Research and Economy and National Foundation for Research, Technology and Development), and the OMV Group. We also thank Mr. Charles Creissen for performing SEM studies, and Dr. Moritz Kuehnel, Dr. Kristian Dalle, and Mr. Benjamin Martindale for helpful comments.

Keywords: carbon dioxide · electrocatalysis · hybrid materials · manganese · reduction

How to cite: *Angew. Chem. Int. Ed.* **2016**, *55*, 7388–7392
Angew. Chem. **2016**, *128*, 7514–7518

[1] a) L. Chen, Z. Guo, X.-G. Wei, C. Gallenkamp, J. Bonin, E. Anxolabéhère-Mallart, K.-C. Lau, T.-C. Lau, M. Robert, *J. Am. Chem. Soc.* **2015**, *137*, 10918–10921; b) A. Taheri, L. A. Berben, *Inorg. Chem.* **2016**, *55*, 378–385.

[2] a) J. Hawecker, J.-M. Lehn, R. Ziessel, *J. Chem. Soc. Chem. Commun.* **1984**, 328–330; b) P. Kang, Z. Chen, A. Nayak, S. Zhang, T. J. Meyer, *Energy Environ. Sci.* **2014**, *7*, 4007–4012; c) S. Lin, C. S. Diercks, Y.-B. Zhang, N. Kornienko, E. M. Nichols, Y. Zhao, A. R. Paris, D. Kim, P. Yang, O. M. Yaghi, C. J. Chang, *Science* **2015**, *349*, 1208–1213.

[3] a) M. Bourrez, M. Orio, F. Molton, H. Vezin, C. Duboc, A. Deronzier, S. Chardon-Noblat, *Angew. Chem. Int. Ed.* **2014**, *53*, 240–243; *Angew. Chem.* **2014**, *126*, 244–247; b) C. Riplinger, M. D. Sampson, A. M. Ritzmann, C. P. Kubiak, E. A. Carter, *J. Am. Chem. Soc.* **2014**, *136*, 16285–16298.

[4] a) C. H. Lee, M. W. Kanan, *ACS Catal.* **2015**, *5*, 465–469; b) T. N. Huan, E. S. Andreiadis, J. Heidkamp, P. Simon, E. Derat, S. Cobo, G. Royal, A. Bergmann, P. Strasser, H. Dau, V. Artero, M. Fontecave, *J. Mater. Chem. A* **2015**, *3*, 3901–3907; c) S. Zhang, P. Kang, T. J. Meyer, *J. Am. Chem. Soc.* **2014**, *136*, 1734–1737.

[5] a) C. D. Windle, E. Reisner, *Chimia* **2015**, *69*, 435–441; b) I. Hod, M. D. Sampson, P. Deria, C. P. Kubiak, O. K. Farha, J. T. Hupp, *ACS Catal.* **2015**, *5*, 6302–6309; c) S. Aoi, K. Mase, K. Ohkubo, S. Fukuzumi, *Chem. Commun.* **2015**, *51*, 10226–10228.

[6] a) T. Atoguchi, A. Aramata, A. Kazusaka, M. Enyo, *J. Electroanal. Chem.* **1991**, *318*, 309–320; b) N. Elgrishi, S. Griveau, M. B. Chambers, F. Bedioui, M. Fontecave, *Chem. Commun.* **2015**, *51*, 2995–2998; c) C. M. Lieber, N. S. Lewis, *J. Am. Chem. Soc.* **1984**, *106*, 5033–5034.

[7] a) A. R. Guadalupe, D. A. Usifer, K. T. Potts, H. C. Hurrell, A.-E. Mogstad, H. D. Abruña, *J. Am. Chem. Soc.* **1988**, *110*, 3462–3466; b) T. R. O'Toole, L. D. Margerum, T. D. Westmoreland, W. J. Vining, R. W. Murray, T. J. Meyer, *J. Chem. Soc. Chem. Commun.* **1985**, 1416–1417.

[8] T. Yoshida, K. Tsutsumida, S. Teratani, K. Yasufuku, M. Kaneko, *J. Chem. Soc. Chem. Commun.* **1993**, 631–633.

[9] Z. Chen, J. J. Concepcion, J. W. Jurss, T. J. Meyer, *J. Am. Chem. Soc.* **2009**, *131*, 15580–15581.

[10] a) M. Bourrez, F. Molton, S. Chardon-Noblat, A. Deronzier, *Angew. Chem. Int. Ed.* **2011**, *50*, 9903–9906; *Angew. Chem.* **2011**, *123*, 10077–10080; b) M. D. Sampson, A. D. Nguyen, K. A. Grice, C. E. Moore, A. L. Rheingold, C. P. Kubiak, *J. Am. Chem. Soc.* **2014**, *136*, 5460–5471; c) C. W. Machan, C. J. Stanton III, J. E. Vandezande, G. F. Majetich, H. F. Schaefer III, C. P. Kubiak, J. Agarwal, *Inorg. Chem.* **2015**, *54*, 8849–8856; d) J. Agarwal, C. J. Stanton III, T. W. Shaw, J. E. Vandezande, G. F. Majetich, A. B. Bocarsly, H. F. Schaefer III, *Dalton Trans.* **2015**, *44*, 2122–2131.

[11] a) J. Hawecker, J.-M. Lehn, R. Ziessel, *Helv. Chim. Acta* **1986**, *69*, 1990–2012; b) C. D. Windle, M. W. George, R. N. Perutz, P. A. Summers, X. Z. Sun, A. C. Whitwood, *Chem. Sci.* **2015**, *6*, 6847–6864.

[12] M. D. Sampson, C. P. Kubiak, *J. Am. Chem. Soc.* **2016**, *138*, 1386 – 1393.
[13] a) J. J. Walsh, G. Neri, C. L. Smith, A. J. Cowan, *Chem. Commun.* **2014**, *50*, 12698 – 12701; b) J. J. Walsh, C. L. Smith, G. Neri, G. F. S. Whitehead, C. M. Robertson, A. J. Cowan, *Faraday Discuss.* **2015**, *183*, 147 – 160.
[14] E. Torralba-Peñalver, Y. Luo, J.-D. Compain, S. Chardon-Noblat, B. Fabre, *ACS Catal.* **2015**, *5*, 6138 – 6147.
[15] J. Willkomm, K. L. Orchard, A. Reynal, E. Pastor, J. R. Durrant, E. Reisner, *Chem. Soc. Rev.* **2016**, *45*, 9 – 23.
[16] C. D. Windle, E. Pastor, A. Reynal, A. C. Whitwood, Y. Vaynzof, J. R. Durrant, R. N. Perutz, E. Reisner, *Chem. Eur. J.* **2015**, *21*, 3746 – 3754.
[17] a) A. Bachmeier, V. C. C. Wang, T. W. Woolerton, S. Bell, J. C. Fontecilla-Camps, M. Can, S. W. Ragsdale, Y. S. Chaudhary, F. A. Armstrong, *J. Am. Chem. Soc.* **2013**, *135*, 15026 – 15032; b) T. E. Rosser, M. A. Gross, Y.-H. Lai, E. Reisner, *Chem. Sci.* **2016**, in print (DOI: 10.1039/C5SC04863J).
[18] G. Neri, J. J. Walsh, C. Wilson, A. Reynal, J. Y. C. Lim, X. Li, A. J. P. White, N. J. Long, J. R. Durrant, A. J. Cowan, *Phys. Chem. Chem. Phys.* **2015**, *17*, 1562 – 1566.
[19] F. Hartl, T. Mahabiersing, P. Le Floch, F. Mathey, L. Ricard, P. Rosa, S. Záliš, *Inorg. Chem.* **2003**, *42*, 4442 – 4455.
[20] G. Redmond, D. Fitzmaurice, *J. Phys. Chem.* **1993**, *97*, 1426 – 1430.
[21] a) C. Costentin, S. Drouet, M. Robert, J.-M. Savéant, *Science* **2012**, *338*, 90 – 94; b) V. V. Pavlishchuk, A. W. Addison, *Inorg. Chim. Acta* **2000**, *298*, 97 – 102.
[22] a) E. S. Donovan, B. M. Barry, C. A. Larsen, M. N. Wirtz, W. E. Geiger, R. A. Kemp, *Chem. Commun.* **2016**, *52*, 1685 – 1688; b) B. A. Johnson, S. Maji, H. Agarwala, T. A. White, E. Mijangos, S. Ott, *Angew. Chem. Int. Ed.* **2016**, *55*, 1825 – 1829; *Angew. Chem.* **2016**, *128*, 1857 – 1861; c) J. D. Froehlich, C. P. Kubiak, *Inorg. Chem.* **2012**, *51*, 3932 – 3934.
[23] a) B. J. Brennan, M. J. Llansola Portolés, P. A. Liddell, T. A. Moore, A. L. Moore, D. Gust, *Phys. Chem. Chem. Phys.* **2013**, *15*, 16605 – 16614; b) F. Li, K. Fan, B. Xu, E. Gabrielsson, Q. Daniel, L. Li, L. Sun, *J. Am. Chem. Soc.* **2015**, *137*, 9153 – 9159.
[24] a) F. Lakadamyali, A. Reynal, M. Kato, J. R. Durrant, E. Reisner, *Chem. Eur. J.* **2012**, *18*, 15464 – 15475; b) N. M. Muresan, J. Willkomm, D. Mersch, Y. Vaynzof, E. Reisner, *Angew. Chem. Int. Ed.* **2012**, *51*, 12749 – 12753; *Angew. Chem.* **2012**, *124*, 12921 – 12925; c) J. Willkomm, N. M. Muresan, E. Reisner, *Chem. Sci.* **2015**, *6*, 2727 – 2736.
[25] a) H. Takeda, H. Koizumi, K. Okamoto, O. Ishitani, *Chem. Commun.* **2014**, *50*, 1491 – 1493; b) T. Van der Graaf, R. M. J. Hofstra, P. G. M. Schilder, M. Rijkhoff, D. J. Stufkens, J. G. M. Van der Linden, *Organometallics* **1991**, *10*, 3668 – 3679.
[26] H. Fei, M. D. Sampson, Y. Lee, C. P. Kubiak, S. M. Cohen, *Inorg. Chem.* **2015**, *54*, 6821 – 6828.
[27] C.-Y. Lin, D. Mersch, D. A. Jefferson, E. Reisner, *Chem. Sci.* **2014**, *5*, 4906 – 4913.

Received: January 29, 2016
Published online: April 25, 2016

